Available online at www.sciencedirect.com
ScienceDirect
Journal of Power Sources 159 (2006) 1310–1315
JOURNAL OF POWER SOURCES
www.elsevier.com/locate/jpowsour

Synthesis, structural and electrochemical properties of pulsed laser deposited Li(Ni,Co)O_2 films

C.V. Ramana [a], K. Zaghib [b,*], C.M. Julien [c]

[a] *Nanoscience and Surface Chemistry Research Group, Department of Geological Sciences, University of Michigan, Ann Arbor, MI 48109, USA*
[b] *Institut de Recherches d'Hydro-Québec, 1800 Boul. Lionel-Boulet, Varennes, Qué., Canada J3X 1S1*
[c] *Institut des Nano-Sciences de Paris, CNRS-UMR 7588, Université Pierre et Marie Curie Campus Boucicaut, 140 rue de Lourmel, 75015 Paris, France*

Received 12 September 2005; received in revised form 2 November 2005; accepted 16 November 2005
Available online 4 January 2006

Abstract

We report the epitaxial growth of the $LiNi_{1-y}M_yO_2$ films (M = Co, Co–Al) on heated nickel foil using pulsed laser deposition in oxygen environment from lithium-rich targets. The structure and morphology was characterized by X-ray diffractometry, electron scanning microscopy and Raman spectroscopy. Data reveal that the formation of oriented films is dependent on two important parameters: the substrate temperature and the gas pressure during ablation. The charge–discharge process conducted in Li-microcells demonstrates that effective high specific capacities can be obtained with films 1.35 μm thick. Stable capacities of 83 and 92 μAh cm^{-2} μm are available in the potential range 4.2–2.5 V for $LiNi_{0.8}Co_{0.2}O_2$ and $LiNi_{0.8}Co_{0.15}Al_{0.05}O_2$ films, respectively. The self-diffusion coefficient of Li ions determined from galvanostatic intermittent titration experiments is found to be 4×10^{-12} cm^2 s^{-1}.

Keywords: Lithium microbatteries; Li(Ni,Co)O_2; Thin films; Pulsed laser deposition

1. Introduction

There is a constantly increasing demand for miniaturized high energy density batteries to power microsystems such as microsensors, smart cards, implantable medical devices, intelligent labels, and so on. In this respect, there has been particular interest in solid-state lithium batteries fabricated by thin-film technology which is also used to produce the microelectronics [1,2]. For all these systems, electrochemical requirements are better expressed by unit surface area. Typical values are in the range 50–150 μAh cm^{-2} μm. On Sept. 6, 2005, Oak Ridge Micro-Energy Inc. announced successful completion of the first manufacturing run of thin-film lithium batteries. Their Li//$LiCoO_2$ microcells deliver 120 μAh cm^{-2} at current density 20 μA cm^{-2} and are unaffected by heating at 300 °C due to the use of highly stable solid-state electrolyte.

Since the lithium intercalation ability of $LiCoO_2$ has been discovered by Goodenough [3] and has been exploited by Sony with the introduction of their Li-ion battery on the market [4], extensive studies has been conducted to develop alternative materials such the solid solution system, especially composition $LiNi_{0.8}Co_{0.2}O_2$ which is expected to form the next-generation electrode, after $LiCoO_2$ [5].

Pulsed laser deposition (PLD) is a successful method in the growth of materials containing volatile components with complex stoichiometries [6–8]. Now, it is well known that the PLD process helps to maintain the stoichiometry of the films primarily because of the rapid ablation process and the relatively high partial pressure of the oxygen in the chamber [9–12]. We are only aware of a few attempts to prepare $LiCoO_2$–$LiNiO_2$ thin films. Wang et al. used PLD technique to grow $LiNi_{0.8}Co_{0.2}O_2$ films on nickel substrate delivering a reasonable capacity of 60 μAh cm^{-2} μm and good capacity retention [13].

In this work, we report on the preparation and characterization of $LiCoO_2$–$LiNiO_2$ thin films grown by the PLD technique from lithium-rich targets. LNC:Al films are grown in the view of powering medical microsensors which requires a low current of few 10 nA. Samples with nominal composition $LiNi_{0.8}Co_{0.2}O_2$ (LNC) and $LiNi_{0.8}Co_{0.15}Al_{0.05}O_2$ (LNC:Al) are fabricated onto heated nickel substrates. The structure and mor-

* Corresponding author. Tel.: +1 450 652 8019; fax: +1 450 652 8424.
E-mail address: zaghib.karim@ireq.ca (K. Zaghib).

0378-7753/$ – see front matter © 2005 Elsevier B.V. All rights reserved.
doi:10.1016/j.jpowsour.2005.11.065

phology were characterized by X-ray diffractometry (XRD), electron scanning microscopy (SEM) and Raman scattering (RS) spectroscopy. The electrochemical behavior of the films has been investigated using galvanostatic titration in lithium cell.

2. Experimental

Thin films of the $LiNi_{0.8}Co_{0.2}O_2$ and $LiNi_{0.8}Co_{0.15}Al_{0.05}O_2$ oxides were prepared using the PLD chamber reported previously [14]. The lithium-rich targets optimized for 15 Li_2O mol% were prepared from powders pressed at 1.5–5 t cm^{-2} and sintered at 800 °C for 24 h. The films were deposited onto silicon (1 1 1) and nickel substrates heated in the temperature (T_S) range 50–500 °C. The energy and the repetition rate of the laser pulse were 300 mJ and 10 Hz, respectively. The chamber base pressure was 1×10^{-6} Torr prior to deposition. The PLD chamber was backfilled with pure oxygen to the total pressure $p(O_2)$ maintained in the range 50–150 mTorr during deposition.

XRD patterns of PLD films were carried out using a Philips X'Pert PRO MRD (PW3050) diffractometer equipped with a Cu anticathode (Cu Kα radiation λ = 1.54056 Å) at room temperature. The surface morphology of the films was observed with a scanning electron microscope (Philips XL30). RS spectra were recorded using the 514.5 nm line of an Ar^+ ion laser (Coherent Radiation) at a power level of 10 mW in a backscattering configuration. The scattered light was analyzed with a Jobin–Yvon U1000 double monochromator and detected with a PMT coupled to a standard photon counting system.

Electrochemical measurements were carried out on Li/$LiClO_4$ in PC/LNC cells with a lithium metal foil as negative electrode and a crystallized film as positive electrode of 1.5 cm^2 active area using a Teflon home-made cell hardware. The Ni substrate was covered by insulating epoxy leaving only the PLD film as active area. Electrochemical titration was made by charging and discharging the cells using the galvanostatic mode of a Mac-Pile system in the potential range between 2.5 and 4.3 V. Quasi open-circuit voltage profiles were recorded using current pulses of 14 μA cm^{-2} supplied for 1 h followed by a relaxation period of 0.5 h. Specific capacity was expressed per unit surface and thickness that is more convenient for thin electrodes. The relation between the gravimetric capacity, C_m, of the material and the specific volumetric capacity of a film, C_f, is given by

$$C_f = 0.36 d C_m \quad (1)$$

where C_f is expressed in mC cm^{-2} μm (or μAh cm^{-2} μm), C_m in mAh g^{-1} and d is the density of the material in g cm^{-3}. Assuming that $LiNi_{0.8}Co_{0.2}O_2$ films have no porosity, with a theoretical density of 4.8 g cm^{-3}, the theoretical gravimetric capacity 274 mAh g^{-1} corresponds to a specific volumetric capacity C_f = 135 μAh cm^{-2} μm which is the value when all Li-ions are extracted (x = 1) from the $Li_{1-x}Ni_{0.8}Co_{0.2}O_2$ host lattice.

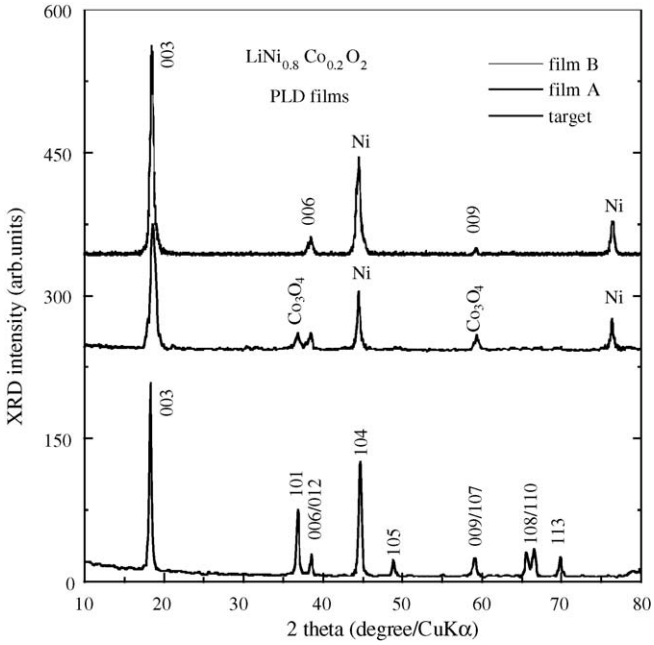

Fig. 1. XRD patterns of pulsed laser-deposited $LiNi_{0.8}Co_{0.2}O_2$ film grown at $p(O_2)$ = 150 mTorr onto Ni substrate at T_S = 450 °C. Curves correspond to the diagram of film grown with 15Li_2O mol% additive in the target (upper curve), film grown without additive (middle), and pattern of the target powders (lower curve).

3. Results and discussion

Fig. 1 shows the XRD patterns of pulsed laser deposited $LiNi_{0.8}Co_{0.2}O_2$ films grown in $p(O_2)$ = 100 mTorr atmosphere onto Ni substrate at T_S = 450 °C. The curves correspond to the diagram of the film grown using 15 Li_2O mol% additive in the target (upper curve), patterns of the film grown without additive (mid-curve) and the XRD diagram of the target powders (lower curve). The X-ray diagram of $LiNi_{0.8}Co_{0.2}O_2$ film formed at low T_S exhibit the amorphous nature of the layer. Similar to the case of $LiCoO_2$, typical peaks of the polycrystalline phase appear upon increasing the substrate temperature (T_S > 200 °C) in oxygen partial pressure $p(O_2)$ = 100 mTorr using a lithium-rich target [9]. The XRD diagram of the $LiNi_{0.8}Co_{0.2}O_2$ film grown onto silicon wafer maintained at T_S = 450 °C in $p(O_2)$ = 100 mTorr from a target without Li_2O additive displays peaks due to the presence of a second phase identified as Co_3O_4. As the amount of Li_2O increased in the target up to 15 mol%, the XRD patterns develop features expected for the regular $LiNi_{0.8}Co_{0.2}O_2$ layered phase. All other peaks in the film data are attributed to the Ni substrate; there is no evidence of either NiO or Co_3O_4 which could be expected from Li-deficient film. The 2θ values of all reflections observed match those in the reference spectrum indexed in the $R\bar{3}m$ system. We observe unambiguously dominant peaks attributed to the (0 0 l), which indicate a strong preferred orientation. Polycrystalline films with preferred orientation have been also obtained with rf-sputtered $LiCoO_2$ on silicon substrates. The high texture is attributed to the tendency to minimize volume strain energy for the thicker films or the surface energy for the very thin films [15]. In the case of the rf-sputtered film,

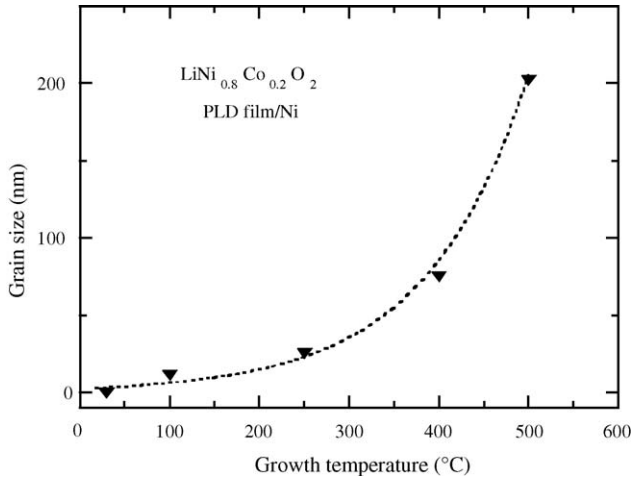

Fig. 2. Particle size as a function of the growth temperature for PLD $LiNi_{0.8}Co_{0.2}O_2$ films deposited onto Ni foil. The dashed line represents the fit of the data to an exponential growth using Eq. (2).

the (1 1 0) lattice plane reflection showed the highest intensity, while in the case of PLD film the (0 0 3) reflection is the major diffraction peaks. This orientation with the (0 0 *l*) planes parallel to the substrate surface shows that the *c*-axis of the unit cell is normal to the film surface. For $LiNi_{0.8}Co_{0.2}O_2$ film, the (0 0 3) diffraction peak at $2\theta = 18.83^\circ$ corresponds to a *d*-spacing of 4.71 Å.

The average grain size of $LiNi_{0.8}Co_{0.2}O_2$ films deposited onto Ni foil was calculated by using the Scherrer's relationship. Fig. 2 displays the variation of the particle size as a function of the growth temperature. The increase in grain size as a result of further increase in T_S beyond 200 °C can be attributed to the enhanced diffusion rate of impinging species on the surface. Thus the grain size is directly related to the surface diffusion similar to diffusion coefficient which can be expressed as

$$L = L_0 \exp\left(\frac{-Q_d}{k_B T_S}\right), \quad (2)$$

where Q_d is the activation energy, k_B the Boltzmann constant, T_S the absolute temperature, and L_0 is a pre-exponential factor that depends on the physical properties of the substrate-deposit. The dashed line (Fig. 3) represents the fit of the data to an exponential growth using Eq. (2). The value $Q_d = 19$ meV is obtained for PLD $LiNi_{0.8}Co_{0.2}O_2$ films.

The morphology surface scanning was done for Li–Ni–Co oxide films. Fig. 3 shows the SEM images of $LiNi_{0.8}Co_{0.2}O_2$ (picture a) and $LiNi_{0.8}Co_{0.15}Al_{0.05}O_2$ (curve b) films deposited onto nickel foil at $T_S > 400$ °C. We can clearly see that the film surface is relatively smooth with an average grain size of 100 nm. As already shown in pictures (4a) and (4b), the layer deposited in $p(O_2) \geq 100$ mTorr ambient develop porous morphology built by particles with spherical shape with a narrow distribution of the grain size. The marked decrease in the particle size of Al-doped oxides is then unequivocally correlated with kinetics of grain formation. Different possibilities can be considered: (i) the conditions under which condensation of the precursor species take place, (ii) the fast kinetics of grain formation with the PLD

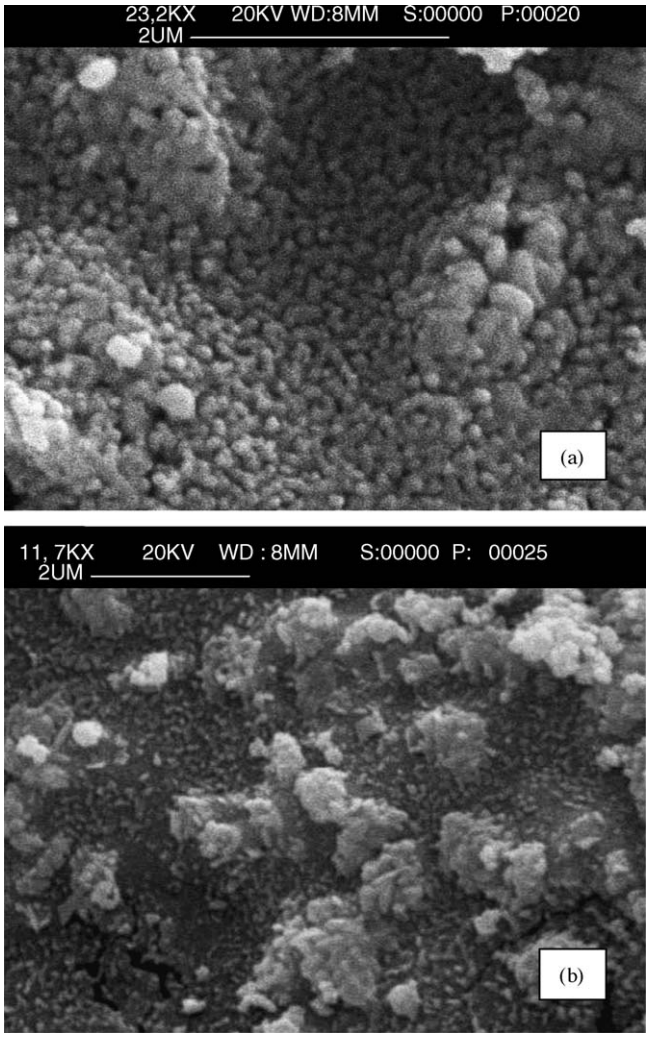

Fig. 3. SEM images of Li–Ni–Co films grown by pulsed laser deposition onto nickel foil. (a) $LiNi_{0.8}Co_{0.2}O_2$ deposited at $T_S = 450$ °C and (b) $LiNi_{0.8}Co_{0.15}Al_{0.05}O_2$ deposited at $T_S = 500$ °C.

deposition, (iii) the limiting effect of aluminium for the growth of particles, and (iv) the effect due to aluminium environment during the condensation process.

The structural modifications at the various stages of pulsed-laser deposition have been investigated by Raman spectroscopy which appears to be a powerful tool for the determination of the lattice symmetry [16]. This technique is particularly useful to distinguish the local environment, e.g. difference between low-temperature and high-temperature phase of $LiCoO_2$-type lattice. Fig. 4 shows the Raman scattering spectra of pulsed laser-deposited $LiNi_{0.8}Co_{0.15}Al_{0.05}O_2$ films prepared onto heated Si substrate at (a) $T_S = 250$ °C and (b) $T_S = 450$ °C in $p(O_2) = 150$ mTorr ambient. Raman peak of the silicon substrate (at 520 cm^{-1}) can be used as an internal standard for estimation of the Raman efficiency of the films.

The RS spectrum of the film grown at $T_S = 450$ °C displays the two Raman-active modes, A_{1g} and E_g, predicted by the theoretical factor-group analysis of the $R\bar{3}m$ rock-salt structure. The RS peaks at 478 and 587 cm^{-1} match well with allowed Raman modes reported for the $0.8LiNiO_2$–$0.2LiCoO_2$ solid

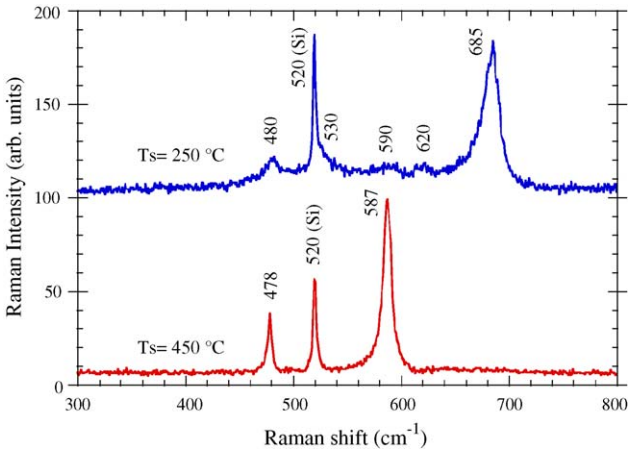

Fig. 4. Raman scattering spectra of pulsed laser-deposited $LiNi_{0.8}Co_{0.2}O_2$ films prepared onto Si substrate heated at (a) $T_S = 250\,^{\circ}C$ and (b)$T_S = 450\,^{\circ}C$ in $p(O_2) = 150$ mTorr ambient. The film grown at low temperature ($T_S = 250\,^{\circ}C$) shows clearly the typical spectrum of the spinel phase (*Fd3m* space group). Raman peak of the silicon substrate (at 520 cm^{-1}) can be used as an internal standard for estimation of the Raman efficiency of the films.

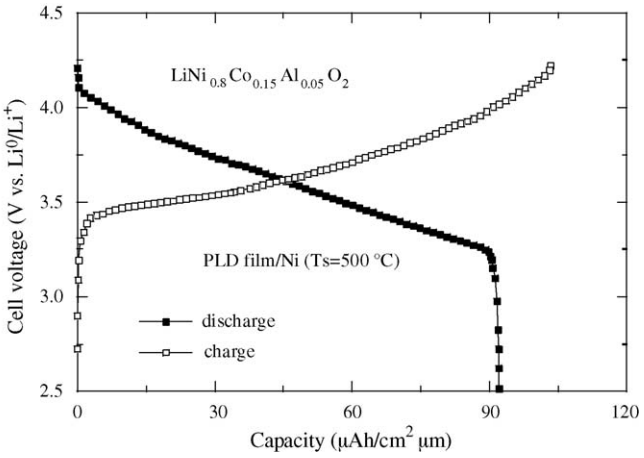

Fig. 6. The initial charge–discharge capacity curves for $LiNi_{0.8}Co_{0.15}Al_{0.05}O_2$ film grown in $p(O_2) = 150$ mTorr ambient onto Ni substrate heated at $T_S = 500\,^{\circ}C$.

solution [16]. The RS spectrum of the film prepared at the low-temperature $T_S = 250\,^{\circ}C$ exhibits various spectral features which correspond to those of a spinel framework. It is well known that $LiCoO_2$ synthesized at low-temperature (LT) adopts the cubic structure which is related to the $Li_2Ti_2O_4$ spinel lattice [17]. The film grown at low temperature ($T_S = 250\,^{\circ}C$) shows clearly the typical spectrum of the spinel phase (*Fd3m* space group) which undergoes a high number of vibration modes due to the lower symmetry. The vibrational signature of the LT-$LiNi_{0.8}Co_{0.15}Al_{0.05}O_2$ consists in a series of broad bands located at 480, 530, 590, 620 and 685 cm^{-1}.

The LNC and LNC:Al oxide films grown onto nickel foil were used as positive electrode materials and tested in a lithium microbatteries with 1 M $LiClO_4$ in propylene carbonate as electrolyte and lithium metal as negative electrode. Typical charge–discharge curves of Li//$LiNi_{0.8}Co_{0.2}O_2$ and Li//$LiNi_{0.8}Co_{0.15}Al_{0.05}O_2$ cells are shown in Figs. 5 and 6,

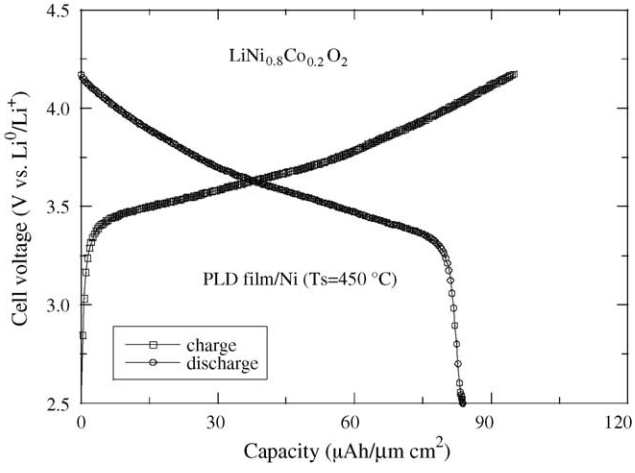

Fig. 5. The initial charge–discharge capacity curves for $LiNi_{0.8}Co_{0.2}O_2$ film grown in $p(O_2) = 150$ mTorr ambient onto nickel substrate heated at $T_S = 450\,^{\circ}C$.

respectively. Electrochemical measurements was carried out at a rate *C*/30 in the potential range 2.5–4.2 V; as such, the voltage profile should provide a close approximation to the open-circuit voltage (OCV). From the electrochemical features, we may make some general remarks as follows: (i) an initial voltage about 2.6 V versus Li^0/Li^+ was measured for Li–Ni–Co oxide film electrodes, which is close to that recorded on the galvanic cell using crystalline material [18]; (ii) the cell-voltage profiles display the typical profile currently observed for $Li_xNi_{1-y}Co_yO_2$ materials [19]; (iii) the cell voltage is a function of the structural arrangement in the film and thus depends strongly on the substrate deposition temperature for $T_S < 300\,^{\circ}C$. Potentials slightly increased for films grown at high substrate temperature. This is consistent with many literature data and ensures that at $T_S = 300\,^{\circ}C$ the material particles are electrochemically active.

Fig. 7a and b gives the incremental capacity curve $(-\partial x/\partial V)$ versus cell voltage for the $LiNi_{0.8}Co_{0.2}O_2$ and $LiNi_{0.8}Co_{0.15}Al_{0.05}O_2$ thin-film, respectively. The electrochemical process seems to be a classical intercalation mechanism for the lithium ions into the Li(Ni,Co)O_2 matrix as indicated by the peaks close to that observed in CV data. The graphs presented in Fig. 7 show clearly the set of well-defined capacity peak at 3.5 and 3.4 V versus Li^0/Li^+ attributed to the redox process of Ni^{3+} to Ni^{4+}. The PLD LNC and LNC:Al oxide films grown at $T_S > 400\,^{\circ}C$ have interesting electrochemical properties for the microbattery application. Such cells deliver a specific capacity of 83 and 92 μAh cm^{-2} μm, respectively. These values could be compared with the theoretical specific capacity of 136 μAh cm^{-2} μm (490 mC cm^{-2} μm) for $LiNi_{0.8}Co_{0.2}O_2$ film assuming a density 4.8 g cm^{-3} and a theoretical gravimetric capacity 274 mAh g^{-1} for a total extraction of Li^+ ions from the host matrix [20].

The kinetics of Li^+ ions in PLD oxide films are important factors in the battery operation since they govern the intercalation/deintercalation rate. The high insertion capability has been confirmed also by measuring the chemical diffusion coefficients of Li^+ ions in $LiNi_{0.8}Co_{0.15}Al_{0.05}O_2$ film grown onto Ni substrate heated at 500 °C in $p(O_2) = 150$ mTorr ambient (Fig. 8).

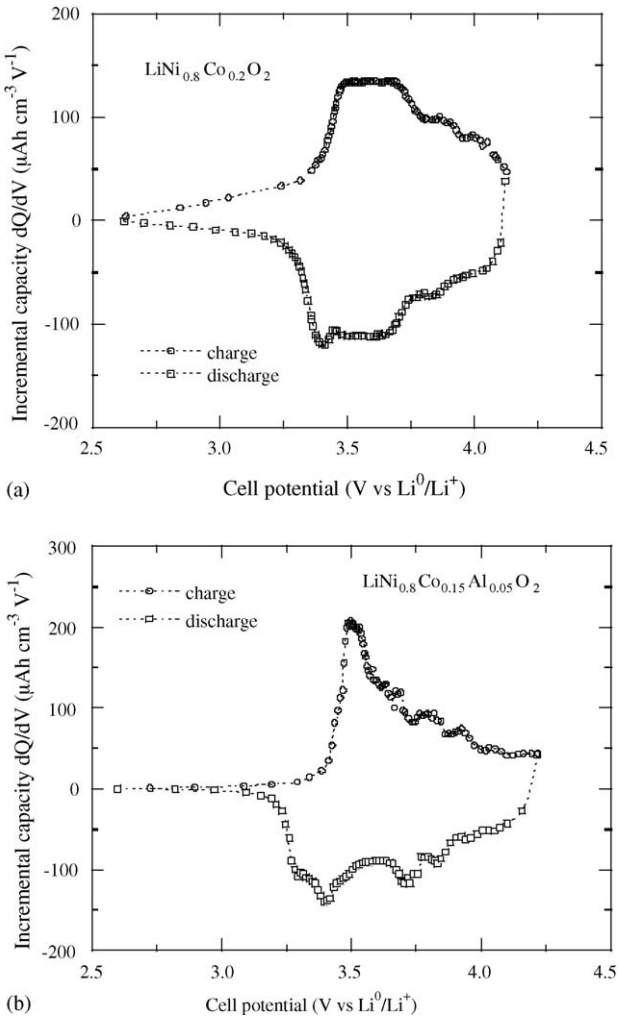

Fig. 7. The incremental capacity (dQ/dV) for (a) $LiNi_{0.8}Co_{0.2}O_2$ film grown at $T_S = 450\,^{\circ}C$ and (b) $LiNi_{0.8}Co_{0.15}Al_{0.05}O_2$ film grown at $T_S = 500\,^{\circ}C$.

The galvanostatic intermittent titration technique (GITT) has been employed to estimate the chemical diffusion coefficients, D^*_{Li}. For short times and small current pulses, the solution of the infinite diffusion problem, based on the early work of Weppner and Huggins [22], leads to a simple expression for the chemical diffusivity of lithium ions if the pulse duration, τ_p, is smaller than the characteristic time $\tau = L^2/D^*_{Li}$ for a film of thickness L, as follows

$$D^*_{Li} = \frac{4}{\pi\tau_p}\left(\frac{mV_m}{MA}\right)^2\left(\frac{\Delta E_s}{\Delta E_\tau}\right)^2, \qquad (3)$$

where A is the surface area, and ΔE_τ and ΔE_S are the voltage changes during the current pulse and after the current pulse, respectively. m, M, and V_m are the mass, molecular weight, and partial molar volume of the host oxide, respectively.

Assuming that the transport phenomena in LNC oxide films is dominated by Li ions and electrons, D^*_{Li} can be expressed as a product of D_{Li}, the electronic transference number, t_e, and the thermodynamic factor of Li, W_{Li} [28]. As $LiNi_{0.8}Co_{0.2}O_2$ is

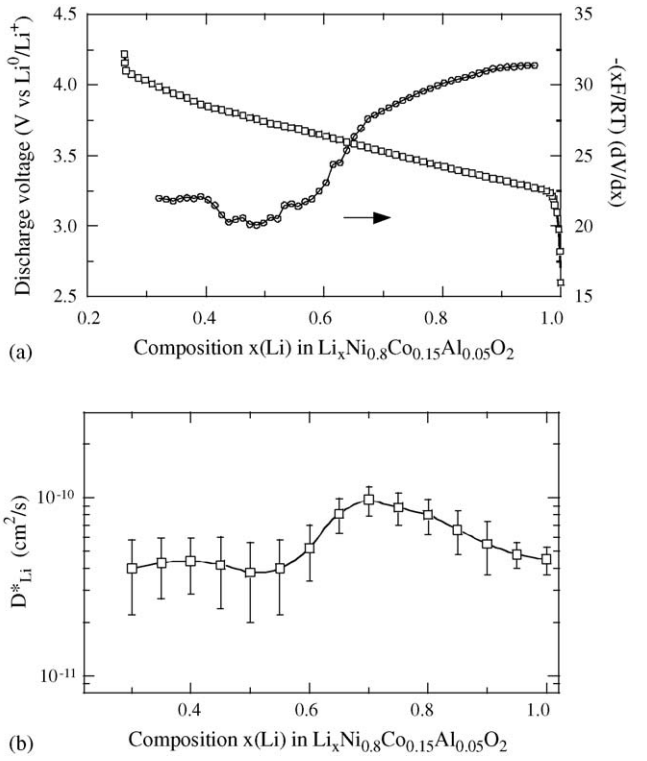

Fig. 8. (a) Plot of the thermodynamic factor vs. lithium composition in PLD $Li_xNi_{0.8}Co_{0.15}Al_{0.05}O_2$ film. (b) Composition dependence of the diffusion coefficient D^*_{Li} of Li-ions.

predominantly an electronic conductor, so that $t_e \approx 1$

$$D^*_{Li} = D_{Li}W_{Li} = D_{Li}\frac{\partial \ln(a_{Li})}{\partial \ln(c_{Li})} = D_{Li}\left(-x\frac{F}{RT}\frac{dV}{dx}\right), \qquad (4)$$

where R is the gas constant, F the Faraday constant and T the absolute temperature. The derivative voltage term ($-dV/dx$) was calculated from the voltage–composition curve shown in Fig. 8a. The faradaic yield $\Delta x = 0.74$ was estimated from practical capacity delivered by the $Li/LiNi_{0.8}Co_{0.15}Al_{0.05}O_2$ cell.

As shown in Fig. 8a, the electrochemical charge process can be attributed to a single-phase reaction because no sharp peak is observed in the ($-dV/dx$) curve, so that Eq. (3) is accurate for the determination of D_{Li}. Fig. 8b shows the chemical diffusion coefficient Li^+ ions in $LiNi_{0.8}Co_{0.15}Al_{0.05}O_2$ film. Results show that the diffusion coefficients for the $LiNi_{0.8}Co_{0.15}Al_{0.05}O_2$ film are in the range 10^{-10} to $10^{-11}\,cm^2\,s^{-1}$ leading a self-diffusivity $D^0_{Li} = 4 \times 10^{-12}\,cm^2\,s^{-1}$. These values are comparable with those reported by Jang et al. [21]. The chemical diffusion coefficient of Li^+ ions increases continuously as lithium ions are extracted from the $LiNi_{0.8}Co_{0.15}Al_{0.05}O_2$ lattice. In this case, the intercalation process is partly controlled by the number of ion occupancies in the host lattice of the crystallite in the film. The increasing values of D^*_{Li} with lithium extraction (decreasing x) is probably due to the lattice expansion.

4. Conclusion

$LiNi_{0.8}Co_{0.2}O_2$ and $LiNi_{0.8}Co_{0.15}Al_{0.05}O_2$ oxide films have been fabricated by pulsed laser deposition at moderate temper-

ature. X-ray powder diffraction and Raman spectroscopy have shown that the conjunction of target composition (lithium-rich), substrate temperature ($T_S > 300\,^{\circ}C$), and partial oxygen pressure $p(O_2) \geq 100$ mTorr promotes reconstruction of a stoichiometric single phase with the layered α-$NaFeO_2$-type structure. Aluminum content increases the interval of thermal stability favoring the formation of nano-structured $LiNi_{0.8}Co_{0.15}Al_{0.05}O_2$ films at moderate temperature. The decreasing particle size upon Al doping is an important trend for the lithium-ion mobility since it reduces the ion diffusion pathway in grains and, thus, the rate capability of the positive electrode considered. Stable capacities of 83 and 92 $\mu Ah\,cm^{-2}\,\mu m$ are available in the potential range 4.2–2.5 V for $LiNi_{0.8}Co_{0.2}O_2$ and $LiNi_{0.8}Co_{0.15}Al_{0.05}O_2$ films, respectively. The self-diffusion coefficient of Li ions determined from galvanostatic intermittent titration experiments is found to be $4 \times 10^{-12}\,cm^2\,s^{-1}$.

References

[1] C. Julien, in: G. Pistoia (Ed.), Lithium Batteries, New Materials, Developments and Perspectives, Elsevier, Amsterdam, 1993, p. 167.
[2] J.L. Souquet, M. Duclot, Solid State Ionics 148 (2002) 375.
[3] K. Mizushima, P.C. Jones, P.J. Wiseman, J.B. Goodenough, Mater. Res. Bull. 15 (1980) 783.
[4] T. Nagaura, K. Tozawa, Prog. Batt. Solar Cells 9 (1990) 209.
[5] M. Wakihara, Mater. Sci. Eng. R 33 (2001) 109.
[6] R.K. Singh, J. Narayan, Phys. Rev. B 41 (1990) 8843.
[7] M. Antaya, J.R. Dahn, J.S. Preston, E. Rossen, J.N. Reimers, J. Electrochem. Soc. 140 (1993) 575.
[8] K.A. Striebel, C.Z. Deng, S.J. Wen, E.J. Cairns, J. Electrochem. Soc. 143 (1996) 1821.
[9] C. Julien, E. Haro-Poniatowski, O.M. Hussain, C.V. Ramana, Ionics 7 (2001) 165.
[10] C. Julien, M.A. Camacho-Lopez, L. Escobar-Alarcon, E. Haro-Poniatowski, Mater. Chem. Phys. 68 (2001) 210.
[11] D. Perkins, C.S. Bahn, J.M. McGraw, P.A. Parilla, D.S. Ginley, J. Electrochem. Soc. 148 (2001) A1302.
[12] D.S. Ginley, J.D. Perkins, J.M. McGraw, P.A. Parilla, M.L. Fu, C.T. Rogers, Mater. Res. Soc. Symp. Proc. 496 (1998) 293.
[13] G. Wang, M.J. Lindsay, M. Ionescu, D.H. Bradhurst, S.X. Dou, H.K. Liu, J. Power Sources 97/98 (2001) 298.
[14] C. Julien, E. Haro-Poniatowski, M.A. Camacho-Lopez, L. Escobar-Alarcon, J. Jimenez-Jarquin, Mater. Sci. Eng. B 72 (2000) 36.
[15] Y.-I. Jang, B.J. Neudecker, N.J. Dudney, Electrochem. Solid-State Lett. 4 (2001) A74.
[16] C. Julien, Solid State Ionics 136/137 (2000) 887.
[17] R.J. Gummow, M.M. Thackeray, W.I.F. David, S. Hull, Mater. Res. Bull. (1994).
[18] A. Castro-Couceiro, S. Castro-Garcia, M.A. Senaris-Rodriguez, F. Soulette, C. Julien, Solid State Ionics 156 (2003) 15.
[19] I. Saadoune, C. Delmas, Solid State Ionics 53–56 (1992) 370.
[20] T. Ozuku, A. Ueda, J. Electrochem. Soc. 141 (1994) 2972.
[21] Y.-I. Jang, B.J. Neudecker, N.J. Dudney, Electrochem. Solid-State Lett. 4 (2001) A74.
[22] W. Weppner, R. Huggins, J. Solid State Chem. 22 (1977) 297.